Velocity and Magnetic Transients Driven by the X2.2 White-Light Flare of 2011 February 15 in NOAA 11158

R. A. Maurya[1,2], P. Vemareddy[1] and A. Ambastha[1]

[1] *Udaipur Solar Observatory, Physical Research Laboratory, Udaipur-313001, India.*

[2] *Astronomy Program, Department of Physics and Astronomy, Seoul National University, Seoul 151-747, Korea.*

ramajor@astro.snu.ac.kr, vema@prl.res.in, ambastha@prl.res.in

ABSTRACT

The first X-class flare of the current solar cycle 24 occurred in Active Region NOAA 11158 during its central meridian passage on 2011 February 15. This two ribbon white-light flare was well observed by the Helioseismic and Magnetic Imager (HMI) on board Solar Dynamics Observatory (SDO). During the peak phase of the flare, we detected magnetic and Doppler velocity transients appearing near the umbral boundary of the main sunspot. These transients persisted for a few minutes and showed spatial and temporal correspondence with the flare kernels. The observed magnetic polarity at the transients' locations underwent sign reversal, together with large enhancement in Doppler velocities. We explain this observational phenomena using the HMI spectral data obtained before, during and after the flare. These changes were reflected in the maps of the AR in all the Stokes parameters. Association of the transient features with various signatures of the flare and the cause and effects of their appearance are also presented on the basis of present theoretical models.

Subject headings: Sun: activity — Sun: flares — Sun: magnetic fields

1. Introduction

It is known that catastrophic changes in the magnetic field configuration of active regions (ARs) at coronal heights trigger energetic explosive events such as flares and coronal mass ejections (CMEs). Therefore, variations in magnetic and Doppler velocity fields are expected to accompany these energetic events. It was first suggested by Giovanelli (1939) that energy release in flares should be associated with observable magnetic field changes. Extensive

efforts have been made since then to detect such changes using photospheric magnetic field observations. Several types of changes in the measured magnetic fields from pre- and post-phases of flares have been reported by ground-based (Patterson & Zirin 1981; Patterson 1984; Wang et al. 1992; Ambastha et al. 1993; Chen et al. 1994; Hagyard et al. 1999), and more recently by space-based (Kosovichev & Zharkova 2001; Qiu & Gary 2003; Wang 2006; Maurya & Ambastha 2008, 2009; Maurya 2010) observations. These changes in observed magnetic fields can be divided into two main categories: "permanent" and "transient". The first type is irreversible change observed during pre- to post- phases of flares. The later, "transient" changes are reversible that occur only during the peak or impulsive phase of energetic events.

The observed changes in magnetic field parameters during the impulsive phase of a flare are, however, expected to be affected by a variety of effects that could introduce ambiguity in the cause and effects of the observed changes. One major concern is that the flare associated modification of spectral line profiles, used for the measurement of photospheric magnetic fields, may lead to incorrect estimation of magnetic fields during the impulsive phase of major flares. Therefore, adequate care must be taken in interpreting the "observed" changes in photospheric magnetic fields and Doppler velocities. For instance, the irreversible changes observed after flares may occur due to flux emergence/cancelation process and may be considered as "real" changes. However, there is ambiguity in interpreting the transients, reversible changes observed during some large flares as it has been difficult to ascertain whether these changes are real or artifacts. These "magnetic transients" are therefore termed also as "magnetic anomalies" (Patterson 1984; Kosovichev & Zharkova 2001; Qiu & Gary 2003; Maurya & Ambastha 2009).

Some numerical experiments have been carried out to confirm magnetic field changes due to a transient change of the spectral line profile from absorption to emission (Machado et al. 1980; Vernazza et al. 1981; Ding & Fang 1989; Ding et al. 2002; Edelman et al. 2004). Effect of line profile change on magnetic field estimation was also reported by Abramenko & Baranovsky (2004) using spectrographic observations of six different photospheric absorption lines at the flare and quiet locations. They showed that the core of spectral profiles at the flare location was shallower as compared to that for the quiet Sun, and less steep in the wings. They attributed the enhanced core emission to thermal heating of photosphere by the flare, and the less steep slope near wings to the inhomogeneity of the photospheric magnetic fields. This resulted in an underestimation of the magnetic field measurements by 18-25% at the flare locations. Qiu & Gary (2003) have reported that sign reversals of magnetic polarity may also be related to non-thermal processes. They found anomalous polarity reversals during a large X5.6 flare of 2001 April 6 at the location of strong hard X-ray (HXR) emission forming near cooler umbral/penumbral regions of the sunspots. These HXR sources are produced by

energetic electron beams impinging at the sites of higher density and strong magnetic fields.

In a recent study (Maurya & Ambastha 2009, hereafter MA09), we had discovered moving transient magnetic and Doppler velocity features during the peak-phases of two major X17/4B and X10/2B white light flares (WLF) of 2003 October 28 and 29, respectively, in NOAA 10486. HXR sources were also observed during these flares. For the flare of 2003 October 28, the HXR sources showed a separation of $\approx$ 23 Mm matching well with the chromospheric Hα flare ribbons. This observation is consistent with the flare models that suggest formation of HXR footpoint sources in the chromosphere or lower corona depending on the energy of penetrating particles. The magnetic and Doppler velocity transients, on the other hand, showed a somewhat greater separation of ≈ 29 Mm similar to the photospheric WLF kernels. At the transients' sites, we detected anomalous magnetic polarity sign reversals during the impulsive phases of these flares. The transients were first detected at the weaker field location of polarity reversal line (PIL), and not in the cooler, stronger magnetic field sites of sunspot umbra/penumbra, as found earlier by Qiu & Gary (2003). However, as the flares in NOAA 10486 progressed, the transients moved away from the PIL towards the stronger fields. We inferred from the analysis of the X17/4B flare of 2003 October 28 that the moving transients were better related to the HXR sources, i.e., the non-thermal processes associated with electron-beam injection, and not to the WLF kernels, i.e., thermal heating.

There have been a very few cases reported so far on the transient magnetic and Doppler velocity features driven by the flares. It appears that these transients may reach detectable levels only in some very energetic, impulsive flares. In this paper, we report the detection of a similar event associated with the first X-class flare of the current solar cycle 24. This two-ribbon WL flare occurred in NOAA AR 11158 during its central meridian passage on 2011 February 15. It was well observed by the Helioseismic and Magnetic Imager (HMI) and Atmospheric Imaging Assembly (AIA) on board Solar Dynamics Observatory (SDO). From the movies of high resolution magnetic and Doppler velocity images, we detected the transients appearing first near the umbral boundary of the main sunspot. It persisted only for a few minutes during the peak phase of the flare. As found earlier in MA09, the magnetic polarity went through a sign reversal at the location of the transients. The Doppler velocity, however, did not show such a sign reversal. Instead, there occurred a large magnitude velocity enhancement at the transient's site.

Using multi-wavelength flare observation from SDO, we intend to study the association of the observed transients with various signatures of the X2.2 flare of 2011 February 15. The spectral data available from SDO-HMI will also be used to investigate the changes in Stokes profiles occurring during the peak phase of the flare. Characteristics of these transients will

be examined to explain their cause and effects using the present theoretical models. The paper is organized as follow: In Section 2, we describe the observational data and methods of analysis. Results and discussions are presented in Section 3. Finally, summary and conclusions are given in the Section 4.

2. Observational Data and Analysis

AR NOAA 11158 was extensively observed by several space borne instruments, such as, HMI (Schou et al. 2012) and AIA (Lemen et al. 2012) on board SDO, Solar Optical Telescope (SOT, Tsuneta et al. 2008) on board Hinode, and Reuven Ramaty High Energy Solar Spectroscopic Imager (RHESSI, Lin et al. 2002). We have used the SOT images to study the flare evolution in the chromosphere along with the spectral, magnetic field and Doppler velocity data obtained from the SDO/HMI.

The HMI observes full solar disk in the photospheric absorption line Fe I centered at the wavelength 6173.3Å and produces images with spatial and temporal resolutions of $0''.5\,\mathrm{pixel}^{-1}$ and 45 s, respectively. HMI magnetograms and Dopplergrams have precisions of 10 G and 13 $\mathrm{m\,s}^{-1}$, respectively. For examining the temporal changes in the Fe I line profile during the period of the flare, we have used the 12 HMI intensity image data taken at six wavelength positions from the line center, ±34.4, ±103.2 and ±172.0 mÅ, in the two circular polarizations. Further, we have obtained the Stokes profiles using the HMI Stokes parameters (I, Q, U and V) at the aforesaid six wavelength positions. The spatial resolution of these parameters is the same as the HMI magnetograms while the temporal cadence is 215 s.

The AIA observes the full Sun in several wavelengths corresponding to various layers of the solar atmosphere: 1700Å (continuum formed in the photosphere and the temperature minimum region at the temperature, $\log T = 3.7$); 304Å (He II formed in the chromosphere and the transition region at the temperature, $\log T = 4.7$); 193Å (Fe XX, XXIV formed in the coronal and hot flare plasmas at the temperature, $\log T = 6.2$, 7.3). The spatial and temporal resolutions of these observations are $0''.6$ pixel^{-1} and 45 s, respectively.

We have used the Ca II H 3968Å line images obtained from the SOT to study the flare kernels at the chromospheric level. The Ca II H line data have spatial and temporal resolutions of $0''.1$ pixel^{-1} and 20 s, respectively. These images were scaled, registered and co-aligned with the corresponding HMI magnetograms.

We extracted $180\times180\,\mathrm{pixel}^2$ areas-of-interest, centered around the AR NOAA 11158 (Carrington longitude 36°, latitude -21°), from the full disk HMI white-light intensitygrams,

magnetograms, dopplergrams, and the AIA images. We also extracted the corresponding line intensity profiles and Stokes vectors. To get images aligned within sub-pixels accuracy, we have used Fourier transform based registration method implemented in the Interactive Data Language (IDL).

The Fourier modulated HXR data during the flare were obtained from the RHESSI data archive (Lin et al. 2002). RHESSI observes the Sun in the energy range 3 keV to 17 MeV, with a spatial resolution of $\sim 2''.3$ in the full Sun field-of-view. We have used the "clean" algorithm implemented under the Solar SoftWare (SSW), to reconstruct the HXR images. The basic method was first developed for radio astronomy by Högbom (1974). It is an iterative algorithm based on the assumption that the image can be well represented by a superposition of point sources. Details of this method to reconstruct the images from the RHESSI data are described in Hurford et al. (2002).

For studying the association of the transients driven by the X2.2 flare with HXR sources, we have constructed the RHESSI HXR images in the energy band 25-50 keV with spatial and temporal resolutions of $4''$ pixel^{-1} and 45 s, respectively, keeping the image center fixed at the position ($205''$, $-222''$). Association of HXR sources with the CaII H flare ribbons and the transients are discussed in the Section 3.3.

3. Results and Discussions

Figures 1 – 10 show the results obtained from the analysis of the observational data for the AR NOAA 11158 during the X2.2 flare of 2011 February 15. In the following, we discuss these results in detail.

3.1. Morphology of AR NOAA 11158 and the X2.2 Flare

AR NOAA 11158 appeared near the disk center at location S19W03 on 2011 February 12 in the rising phase of the current solar cycle 24. Subsequent to its birth on February 12, it evolved very rapidly and quickly developed from a simple β- to a very complex $\beta\gamma\delta$-configuration by 2011 February 15. (A detailed study of the surface and sub-surface evolution of this AR has been undertaken and results therefrom will be communicated in a subsequent paper.)

During its disk transit, NOAA 11158 produced several C-class and 5 M-class flares. It also unleashed the first X-class flare of the current solar cycle observed on 2011 February 15. This event was a two ribbon WLF as seen in HMI white-light images. The flare peaked at

01:56 UT, when the AR was centered around S20W12, and was registered X2.2 magnitude on the Richter scale of solar flares. In Figure 1(top two rows), development of the flare is shown using SOT CaII H filtergrams of the AR NOAA 11158 on 2011 February 15.

The co-aligned, extracted HMI and AIA images of AR NOAA 11158, obtained in different wavelengths during the flare, are shown in Figure 2. The top panel shows the AIA images taken at the rising phase of the flare around 01:46 UT in 1700, 304 and 193Å (from the left to right). These wavelengths correspond to different layers of the solar atmosphere, viz., temperature minimum region, chromosphere and corona, respectively. The bottom panel shows the HMI white-light image, magnetogram and dopplergram taken around the peak phase of the flare at 01:53 UT.

Animations of HMI magnetograms and dopplergrams showed "magnetic" and faint "Doppler" transient features (TFs) appearing near the umbral boundary of the main sunspot during the peak phase of the X2.2 flare. The dotted (dashed) curves labeled by L1 and L2 represent the locations of the TFs during the peak phase of the flare, at 01:53 UT, when the features were prominently seen in the HMI magnetogram. These curves are drawn over the subsequent figures for reference. It is evident from the bottom panel that these transients appeared in rather narrow ridges along the umbral boundaries of the opposite polarity sunspots. The images in the top panel further illustrate that L1-L2 were associated with the flare ribbons observed in different AIA wavelengths.

Profiles of relative mean flare intensity $\Delta I/I$ with respect to the quiet Sun in different AIA wavelengths, obtained from the extracted and co-aligned images, are shown in Figure 3. GOES soft X-ray (SXR) profiles in the wavelength range 1.0-8.0 (0.4-5.0Å) are shown by solid (dotted) curves. RHESSI HXR light curve (dashed) in the energy band 25-50 keV is also shown, which is scaled in the plot range as marked in the left-hand side ordinate. GOES 1.0-8.0Å and GOES 0.4-5.0Å emissions peaked at 01:56:49 and 01:55:50 UT, respectively, while the RHESSI HXR emission peaked a few minutes before, at 01:53:40.

The relative flare intensity profiles obtained in different AIA wavelengths are also plotted in Figure 3, according to the scale given in the right-hand side ordinate. As evident, the flare intensities in the AIA wavelengths of 193, 304 and 1700Å started rising around 01:46:53, 01:44:41 and 01:45:44 UT, and peaked at 01:58, 01:56, 01:54 UT, respectively. The flare decayed, in all the wavelengths, by 02:40 UT, i.e., after one hour of the onset of the flare. It is to note that the AIA emissions, particularly in 304Å, saturated during the peak phase of the flare. Hence it is difficult to precisely identify the flare maximum in these wavelengths. However, it is evident that the AIA intensity profiles showed similar trend as the GOES SXR, while, the HXR profile was much narrower with steep rise and decay phases.

The light curves in different wavelengths follow the standard flare model for energy propagation at different heights in the solar atmosphere (Kane 1974). The general understanding of the flare physics is based on the concept of reconnection of magnetic field lines at coronal heights (Sturrock 1966; Hirayama 1974; Kopp & Pneuman 1976). Energy released during a flare covers a wide range of wavelengths, however, it is easier to observe in certain spectral lines as shown in Figure 3. During the pre-flare stage, where the release of the stored magnetic energy is triggered, the chromospheric flare ribbons are seen easily (see, Figure 1 *top*). The increasing separation of flare ribbon with time results from reconnection of magnetic field lines at successively increasing coronal heights. Further, the energetic particles released in the corona during a flare take increasingly longer time to propagate through the denser layers downwards to the photosphere. This agrees with the observed flare light curves in 304Å which started rising at 01:44:41 UT and thereafter in 1700 Å corresponding to the photosphere and the temperature minimum region. As the flare progressed, the temperature also increased making the flare ribbons visible in higher temperature plasmas in the coronal regions corresponding to the 193Å emission.

3.2. The Magnetic and Doppler Velocity Transients

The observed "magnetic" and "Doppler" TFs appeared during the peak phase of the X2.2 flare of 2011 February 15 (c.f., Figure 2). Similar features were reported earlier during the more energetic X17/4B and X10/2B flares of October 28 and 29, 2003 (Maurya & Ambastha 2008, 2009, 2010a), and the X5.6 flare of 2001 April 6 (Qiu & Gary 2003). Venkatakrishnan et al. (2008) have also reported co-spatial Doppler ribbons associated with the Hα flare ribbons of the X17/4B flare. These TFs, usually located around cooler umbral boundary of the sunspots, were found to be largely co-spatial with the flare ribbons observed at different heights of the solar atmosphere, viz, chromosphere, transition region and corona (see Figures 1, 2).

A time sequence of the consecutive difference images of the HMI magnetograms of AR NOAA 11158 in Figure 1 shows dark patches representing the magnetic transients along the curves L1 and L2. These TFs appeared and faded in a few minutes' period (01:50-02:02 UT) during the impulsive phase of the flare. From Figure 1, it is evident that the transients were co-spatial with the observed CaII H line flare ribbons. However, while the CaII H flare ribbons separated away, the TFs remained nearly stationary with time.

Using an automated method described in Maurya & Ambastha (2010b), we determined that the CaII H flare ribbons separated out with an average velocity of 8 km s^{-1}. This is much smaller as compared to the earlier reported velocities in the range of 50-75 km s^{-1} for

the flare ribbons and the TFs observed during the X17/4B super-flare of 28 October 2003 in NOAA 10486. In that event, the TFs rapidly moved away from the weak field regions of the PIL reaching a maximum separation of around 27.9±0.4 Mm. Another part of the TF observed near the leading sunspot (i.e., strong magnetic field region), on the other hand, remained stationary (MA09). Similarly, the TFs associated with the X10/2B flare of October 29, 2003 in the same AR occurred in the umbral/penumbral region of the following sunspot. Those TFs also remained stationary as observed here in the case of the X2.2 flare of 2011 February 15.

3.2.1. Anomalous Reversal of Magnetic Polarity

We measured magnetic flux and Doppler velocity in AR NOAA 11158 along a horizontal line PQ (Figure 4,*top*) drawn through the location 'A' of the observed TF before and during the flare maximum in order to investigate their variations. The line PQ was selected by plotting the magnetic flux profiles along a horizontal raster moving from the bottom to the top of the selected magnetograms. The profiles of magnetic flux and Doppler velocity along PQ are shown in Figure 4 (*bottom*), where the solid and dashed curves represent the magnetic fluxes/velocities before (01:39:00 UT) and during (01:53:15 UT) the flare maximum, respectively. The magnetic flux profiles during the pre- and peak-phases of the flare matched at all points along PQ except at the location 'A' (see Figure 4c). It gives a clear evidence of an abnormal sign reversal in magnetic flux polarity at 'A' around the peak phase of the flare from the pre-flare phase. The Doppler velocity profiles along PQ obtained during the pre- and peak phase of the flare, however, do not match so well as is the case for the magnetic flux profiles (see Figure 4d). This is mainly due to the effect of solar p-mode oscillations. But, there is also a large increase in the Doppler velocity during the peak phase of the flare at 'A', i.e., the location of sign reversal in magnetic polarity.

What processes caused the observed abnormal magnetic flux sign reversal and the Doppler velocity enhancement? Are they real changes? Or, is it related to line profile change (Ding et al. 2002; Qiu & Gary 2003) or some other process such as the impact of a shock wave (Zharkova & Zharkov 2007) on the Fe I line-production region? More recently, Kosovichev (2011) have reported "sunquake" sources in the regions of TFs and suggested these to arise due to thermal and hydrodynamic effects of high-energy particles heating the lower atmosphere. Apart from the observed transients in magnetic flux and Doppler velocities, increase in the continuum intensity was seen in the form of white-light flare ribbons. Notably, the flares studied in MA09 were also white light events during which similar TFs were detected.

One may attribute the observed sign reversals to the expected change in the spectral line profile from absorption to emission occurring during these large WL flares. However, the non-LTE calculations by Ding et al. (2002) were carried out for the spectral line Ni I 6768Å, used in GONG and MDI instruments for magnetic and Doppler measurements. They showed that this line, formed in thermally stable regions, can turn into emission only by a large increase of electron density and not by heating of the atmosphere by any other means. They suggested that such non-thermal effects are most pronounced in a cool atmosphere where continuum is maintained at low intensity level. The observed flare-associated sign reversal in magnetic flux reported here also occurred in the cooler umbral boundary of the sunspot in agreement with Ding et al. (2002). However, there are also exceptions as reported in the case of the X17/4B flare of October 28, 2003 in NOAA 10486, where the TFs formed in the weak magnetic field regions around the PIL.

If the line formation model given by Ding et al. (2002) for Ni I were to be applicable also to the Fe I line used in the HMI measurement, one would suggest that the observed sign reversal is due to the change in line profile. An observational evidence of the Ni I line profile change was not available for the WL flares previously studied in MA09 due to the lack of spectral data from MDI and GONG. Therefore, our interpretation of the origin of the transients was limited to their spatio-temporal association with WL flare kernels and non-thermal HXR sources. However, as the required spectral data is now available from the HMI for the X2.2 flare studied here, we can look for the observational evidence of any flare related changes in the Fe I line profiles at the location of the TFs. The results are discussed in Section 3.4.

3.2.2. Space-Time Maps of Magnetic flux and Doppler Velocity

In order to study the temporal variations of the TFs, we constructed space-time maps of magnetic flux and Doppler velocity in the AR along the line PQ as shown in Figure 4(*top*). We added corresponding magnetic and Doppler velocity values along PQ during the period 01:38:15–02:15:45 UT of 2011 February 15. We also constructed a similar space-time map for the HMI white-light images.

The space-time maps thus constructed are shown in Figure 5(*top*). Here, the x- and y-axes represent time and longitudinal positions along PQ, respectively. As observed during the period 1:47-2:08 UT, these maps show a clear signature of the magnetic and Doppler transients in the box drawn along the time line EF at the longitude 195″. Magnetic flux (MF) and Doppler velocity (DV) values along the line EF are plotted as dashed-dotted curves in the corresponding bottom panels. The solid (dotted) curves show the integrated GOES-15

SXR flux in the wavelength range 1.0–8.0 (0.5–4.0) Å, while the dashed curves represent the WLF intensity scaled in the left-hand side y-axis.

It is evident from Figure 5(*bottom*) that MF and WLF began rising at 01:47 UT with a delay of one (two) minutes from the rise of the GOES flux in the wavelength range 1.0-8.0(0.4-5.0)Å. However, MF reached its peak much faster, at 01:53:15 UT, as compared to various other flare intensities: WLF at 01:54:00 UT, and GOES SXR 0.4–5.0 (1.0–8.0)Å at 01:55:50 (01:56:49) UT. Similarly, the MF and WLF profiles decayed much faster than the GOES flux. The DV profile also peaked simultaneously with the WLF and MF profiles. Its profile returned back to the original level at 2:00 UT, i.e., about 10 minutes before the magnetic flux. From these time profiles at 'A' (Figure 4, *top*), we thus infer that the observed transients and WLF had similar temporal profiles, reaching their peaks 2-3 min prior to the peaks for the GOES fluxes. Also, the DV profile was comparatively much sharper than the MF profile.

If the MF and DV transients occurred due to line profile changes (Qiu & Gary 2003), then they both are expected to exhibit similar temporal evolution. Similarity of the transient and WLF profiles suggests that thermal heating process may have caused these transients. The time delay between the TFs and GOES SXR peaks indicates the travel time that the energetic charged particles released in corona during the flare took to reach at the photosphere and produce the TFs and subsequent thermal heating giving rise to the soft X-ray flux. We further discuss the spatial and temporal variations of TFs along the curves L1 and L2, and their association with WLF, CaII H and HXR kernels in the following section.

3.3. The White-light, CaII H Flare and the HXR Sources

In order to identify the temporal and spatial association of RHESSI HXR sources and flare ribbons with the TFs, we overlaid the 25-50 keV RHESSI HXR contours on the consecutive magnetogram and dopplergram difference images (Figure 6). The transients are seen in the respective background images in the time period 1:49:57-02:01:12 UT. The HXR contours (dash-dotted) were drawn at 40, 60 and 80% levels of the maxima. These features were observed around the magnetic polarity inversion line (PIL); not drawn here to avoid overcrowding. The CaII H flare ribbons (solid contours) and the transients, i.e., L1 and L2 appear to be well correlated.

The HXR sources evolved both spatially and temporally along L1 and L2 as shown in the panels (a) to (d). The source region of HXR moved toward west, parallel to the magnetic neutral line during the period when the TFs were seen. The observed motion of

HXR sources is attributed to the temporal movement of the reconnection site as reported earlier by Masuda et al. (2001); Bogachev et al. (2005); Zhou et al. (2008). From Figure 6, it is evident that the HXR sources were not very well correlated with the TFs during the entire peak phase of the flare as compared to the CaII H ribbons. Therefore, we infer that HXR sources alone were not the cause or effect of the TFs. This inference agrees with our earlier results obtained for the X10/2B flare of 2003 October 29 (MA09).

Although the WLF ribbons were faintly observable in the HMI continuum animations, they are rather difficult to identify even in the difference images. However, from the animations, the WLF ribbons appeared to be correlated with the TFs. This is further corroborated by the the WLF intensity, magnetic and Doppler velocity profiles of Figure 5(*bottom*).

Qiu & Gary (2003) had reported that (i) the apparent sign reversal occurs in cool, strong-field (>1000 G) regions within sunspot umbrae, (ii) locations of the anomaly are exactly co-aligned with the thick-target HXR sources, and (iii) the transient reversal flux is temporally correlated with the HXR flux. Based on these results, they proposed that at the flare kernels the Ni I absorption line profile is either temporarily turned into emission or significantly broadened with a strong central reversal due to the non-thermal beam impact on the umbral atmosphere. However, our results for this X2.2 flare are not in full conformity with Qiu & Gary (2003) as we did not find a very good association of HXR and TFs. Therefore, the TFs observed during the flare of 2011 February 15, and the X10/2B flare of 2003 October 29 reported in MA09, are not fully explained only by the non-thermal process suggested in Qiu & Gary (2003).

3.4. Line Profile Changes Associated with the Transients

Earlier studies based on numerical models (Machado et al. 1980; Vernazza et al. 1981; Ding & Fang 1989; Ding et al. 2002; Qiu & Gary 2003) have shown that the flare associated transients may be attributed to a change in the spectral line profile. However, due to the non-availability of observational spectral data, the transients could be examined using only the imaged data of the flares at various wavelengths and inferences were drawn based on this indirect method. We are now able to address this issue using SDO/HMI spectral observations. The HMI observes the Sun in two circular polarizations at six wavelength positions ($\pm 34.4, \pm 103.2$ and ± 172.0 mÅ) of the Fe I spectral line. Using these observations one can construct the line profile for any desired location of the full disk Sun. The spectroscopic imaging of HMI observations are described in a recent paper by Martínez Oliveros et al. (2011).

We have already shown the strong spatial association of magnetic transients with the WLF kernels. Figure 7(*top*) shows the consecutive difference magnetogram and white-light images of the AR NOAA 11158 during the peak phase (01:53:15 UT) of the X2.2 flare. We selected a quiet (P_1) and a transient (P_2) location as marked by the arrows. Figure 7(c-d) shows the line profiles at these two locations. Solid (dashed) curve represents the line profile during the pre (peak) phase of the flare. These curves were obtained from a four term Gaussian fitting (except for the peak profile at P_2 where such a fitting was not possible). It is evident that the line profile turned to emission at the wavelength $\Delta\lambda$=-34.4 mÅ and became broader during the peak phase of the flare as compared to the pre-flare phase. This change in the line profile shape is expected to be the main reason for the observed flare associated sign reversal of magnetic flux and the enhancement of Doppler velocity at the location P_2 during the peak phase of the flare. No such change was found at P_1 taken as a reference location far away from the flare.

From the HMI spectral line-profile data, we now attempt to explain the reason for these transients. In the SDO/HMI measurements, magnetogram and Dopplergram maps of the full disk Sun are computed from the phase of the Fourier transform (first component) of the line profile values. The phase is determined for the LCP and RCP components independently, and the Dopplergrams and magnetograms are constructed from the mean and difference, respectively (Schou et al. 2012). However, the standard procedure assumes only a moderate line shift due to Doppler velocity and Zeeman splitting. The regions having large changes in the line profile shape, e.g., line reversal, and large shifts would not be covered by the algorithm, resulting in artifacts in these measurements. For this large X2.2 flare, the spectral line core at the locations of the transient evidently turned from absorption to emission. Therefore, it is difficult to get "correct" values of magnetic flux and Doppler velocity using the above algorithm.

In the following, we have used a two point algorithm to illustrate the result of the observed spectral line reversal at the transient locations. The magnetic flux and Doppler velocity values can be computed from the line intensities in the LCP and RCP as follow: Let $I_i^{\rm LCP,RCP}$, $i = 0, \ldots, 5$ be the line intensities in the two circular polarizations, LCP and RCP, at the six wavelength positions, $\Delta\lambda_i = 68.8\, i - 172.0$, centered around the Fe I spectral line. Then the mean intensities in the blue and red wings of the line can be written as,

$$I_b^{\rm LCP,RCP} = \frac{1}{3}\sum_{i=0}^{2} I_i^{\rm LCP,RCP}$$

and

$$I_r^{\rm LCP,RCP} = \frac{1}{3}\sum_{i=3}^{5} I_i^{\rm LCP,RCP},$$

respectively. The parameters sensitive to magnetic flux (say, ψ_B) and Doppler velocity (say, ψ_V) fields, can be written as,

$$\psi_B = \frac{1}{2}\left[(I_b^{\rm RCP} + I_r^{\rm LCP}) - (I_b^{\rm LCP} + I_r^{\rm RCP})\right]$$

and

$$\psi_V = \frac{1}{2}\left[(I_b^{\rm LCP} + I_b^{\rm RCP}) - (I_r^{\rm LCP} + I_r^{\rm RCP})\right],$$

respectively.

The parameters ψ_B and ψ_V for any location of the AR NOAA 11158 can thus be computed using the 12 line intensity observations at six wavelength positions in the two circular polarizations. However, it is to note that as such these parameters do not represent the magnetic and Doppler velocity fields. They are defined here only to examine the observed magnetic polarity sign reversal and Doppler velocity enhancement at the transients' locations (see Figure 4c, d). Furthermore, this is used to illustrate the observed artifacts in magnetic and Doppler velocity measurements resulting from the standard procedure adopted in SDO/HMI.

The values of the parameters ψ_B and ψ_V at the location P_2 during pre(peak) phase of the flare was found to be -0.034(-0.008) and 0.036(0.054), respectively. It is evident from these computed values that the parameter ψ_B tends towards a positive value during the peak phase of the flare as compared to that in the pre-flare phase. This indicates the reason for the observed sign reversal in the magnetic polarity at location P_2 or at A (see Figure 4c). Similarly, the velocity parameter ψ_V increased during the peak phase of the flare, indicating the large enhancement in the HMI Doppler velocity at P_2 or at A (see Figure 4d).

Figure 8 shows the temporal variation in the normalized line intensities at the six wavelength positions $\pm 34.4, \pm 103.2$ and ± 172.0 mÅ, where panels (a) and (b) correspond to the locations P_1 and P_2, respectively. Panel (a) shows that there was no significant change in the line profile shapes at P_1 from the pre- to peak-phase of the flare. The bottom panel (c) shows the corresponding variation in the RHESSI HXR flux (in the energy range 25-50 keV),

white-light (WL), photospheric magnetic flux (B_p) and Doppler velocity (V_p). The parameters B_p, V_p and WL are normalized to the plot range at the left ordinate axis. The RHESSI HXR fluxes are shown with respect to the right ordinate axis. The shaded area shows the time range of the transients. It is evident from panel (b) that the change in line profile at P_2 is temporally associated with the transients. This is also the period of the peak phase of the flare as seen from panel (c). The spectral line intensity near the core (i.e. at wavelength ± 34.4 mÅ) increased towards the continuum. The intensity enhancement was found to be stronger at the blue wing as compared to that in the red wing. This asymmetry resulted in the enhancement of Doppler velocity in the same sign (Figure 4d) as explained earlier.

From the spectral data available during this flare, it is thus evident that line profile changes occurred during the impulsive phase of the flare. The estimated magnetic flux and Doppler velocity values as obtained by HMI algorithms were affected by these changes during the impulsive phase of the flare, resulting in the observed transient features in magneto(Doppler)grams. It is to note that a purely line-of-sight magnetic field would result in a spectral line with a missing pi-component. Also, the horizontal and vertical gradients in magnetic field can cause asymmetric line profiles. The way to resolve these ambiguities would be to not just look at the LCP and RCP profiles, but all the stokes profiles, i.e., $I \pm U$ and $I \pm Q$. Such profiles are now available from the SDO/HMI. We obtained the required data corresponding to this flare and aligned the Stokes vectors in a similar manner as was done for other data sets of this study. Figure 9 shows the consecutive difference maps of the Stokes parameters (I, Q, U and V) constructed for the AR NOAA 11158 at the six wavelengths during the peak phase of the flare. Strong transient signals are seen in all these Stokes maps, which are particularly more prominent around the Fe I line center (i.e., at -34.4 and 34.4 mÅ).

We have further analyzed the line profiles at several flare and quiet locations of the AR NOAA 11158 for examining the transient changes in the Stokes profiles. These profiles $I \pm U$ and $I \pm Q$ at the transient location P2 are plotted in Figure 10. Solid (dotted) curves correspond to the profiles during pre(peak) phase of the flare. There is a strong reversal at the wavelength -34.4 mÅ away from the line center, similar to the profile derived from the continuum as shown in Figure 7(d). Here it is to note that the magnitude of Stokes I is much larger at all wavelengths compared to the magnitude of Stokes Q and U. Hence, the differences seen in the computed Stokes profiles I±Q and I±U are small.

The observed line profile changes could be related to the thermodynamic change occurring during the flare peak time as the height of line formation can drastically change due to the moderate perturbation of temperature and density. This can be attributed to a large increase of electron density as shown by the non-LTE calculations of Ding et al. (2002)

for the Ni I 6768 Åline. They suggested that the non-thermal excitation and ionization by the penetrating electrons generate a higher electron density which enhances the continuum opacity, thereby pushing the formation height of the line upward. The precipitation of electrons and deposition of energy in the chromosphere, enhanced radiation in the hydrogen Paschen continuum gives rise to the line source function, leading to an increase of the line core emission relative to the far wing and continuum.

4. Summary and Conclusions

We have analyzed the HMI magnetic flux and Doppler velocity images of AR NOAA 11158 obtained during the X2.2 flare of 2011 February 15. We detected transient magnetic and Doppler features during the peak phase of this flare as reported earlier in a few large X-class flares. This transient phenomenon is not well understood as there are questions on their physical mechanism and their association with observed anomalous sign reversal in magnetic polarity, Doppler velocity enhancement, WLF kernels and HXR sources, etc. From the observational data obtained from different instruments, we derived the following important characteristics of these transients driven during the peak phase of the X2.2 flare.

The TFs showed spatial and temporal association with the flare ribbons observed at different heights in the solar atmosphere. They were well correlated also with the WLF kernels. These features occurred near the cooler, umbral/penumbra boundary of the main sunspot. It is to note that the TFs detected in AR NOAA 10486 (MA09) during the X17/4B flare of 2003 October 28 were also associated with WLF kernels, and moved with velocities in the range of 30 to 50 km s^{-1}. The TFs observed during the energetic X2.2 flare of 2011 February 15, however, were observed to be nearly stationary, although the corresponding CaII H line flare ribbons separated out with a mean velocity of 8 km s^{-1} as calculated by an automated method (Maurya & Ambastha 2010b).

The anomalous sign reversal in magnetic polarity during the X2.2 flare of 2011 February 15 was found similar in nature as observed in the AR NOAA 10486 during the X17/4B and X10/2B flares of 2003 October 28 and 29, respectively. It should be noted that the GONG and MDI data for the flares in NOAA 10486 were based on the Ni I line, while the HMI data for the X2.2 flare studied in this paper are based on the Fe I line. Thus, the transient features appearing in the peak phase of major flares seem to be unrelated to the line used in the measurements.

The spectral data available from SDO-HMI provide unambiguous evidence of the changes occurring in the Fe I line and the corresponding Stokes profiles during the impulsive phase

of the flare. The estimated magnetic flux and Doppler velocity values as obtained by HMI algorithms were affected by these changes, resulting in the observed transient features in magneto(Doppler)grams.

This change in the line profile may arise due to both thermal effects and non-thermal excitation and ionization by the penetrating electron jets produced during the large flares. The precipitation of electrons and deposition of energy in the chromosphere gives rise to the line source function leading to an increase of the line core emission relative to the far wing and continuum of the Ni I line, as suggested by Ding et al. (2002).

The magnetic transients were observed at the locations of anomalous sign reversal of magnetic polarity. Co-temporal enhancement in the measured Doppler velocity also occurred there. Qiu & Gary (2003) suggested that the observed sign reversal is caused by changes in the line profile related to the non-thermal effects. But the TFs seen during the X2.2 flare did not show a good correlation with the HXR sources, particularly in the post-peak phase of the flare. Therefore, energetic injection of electrons alone do not appear to have caused the observed changes in the spectral line in this flare. Thermal effects also appear to have contributed to the observed changes as inferred from the observed association of the TFs with the flare ribbons.

We thus conclude that the magnetic and Doppler transients observed during the X2.2 flare of 2011 February 15 were essentially related to the line profile changes. These changes were reflected in the maps of the AR in all the Stokes parameters. However, they did not correspond to a 'real' change occurring in the photospheric magnetic flux or Doppler velocity during the impulsive phase of this, and the other such large, energetic flares. Both thermal and non-thermal physical processes operating during the flare may have contributed to the transient changes in spectral line profiles. Therefore, the observed magnetic and velocity transients may be considered to be the observational signatures of these physical processes occurring during the peak phase of the flare.

This work utilizes data from the Helioseismic and Magnetic Imager (HMI) and the Atmospheric Imaging Assembly (AIA) on board Solar Dynamics Observatory (SDO). This work also utilizes the X-ray data obtained by Ramaty High-Energy Solar Spectroscopic Imager (RHESSI), and CaII H data from the Solar Optical Telescope (SOT) on board Hinode. We are grateful to S. Couvidat of Stanford University for providing the spectral data and helpful discussions. We thank anonymous referee and Professor Jongchul Chae for their valuable comments and suggestions that helped in improving the manuscript. One of the authors (RAM) acknowledges support by the National Research Foundation of Korea (2011-0028102) under which a part of this work was carried out.

REFERENCES

Abramenko, V. I., & Baranovsky, E. A. 2004, Sol. Phys., 220, 81

Ambastha, A., Hagyard, M. J., & West, E. A. 1993, Sol. Phys., 148, 277

Bogachev, S. A., Somov, B. V., Kosugi, T., & Sakao, T. 2005, ApJ, 630, 561

Chen, J., Wang, H., Zirin, H., & Ai, G. 1994, Sol. Phys., 154, 261

Ding, M. D., & Fang, C. 1989, A&A, 225, 204

Ding, M. D., Qiu, J., & Wang, H. 2002, ApJ, 576, L83

Edelman, F., Hill, F., Howe, R., & Komm, R. 2004, in SOHO 14 Helio- and Asteroseismology: Towards a Golden Future, ed. D. Danesy, (ESA SP-559, Noordwijk:ESA), 416

Giovanelli, R. G. 1939, ApJ, 89, 555

Hagyard, M. J., Stark, B. A., & Venkatakrishnan, P. 1999, Sol. Phys., 184, 133

Hirayama, T. 1974, Sol. Phys., 34, 323

Högbom, J. A. 1974, A&AS, 15, 417

Hurford, G. J., et al. 2002, Sol. Phys., 210, 61

Kane, S. R. 1974, in IAU Symposium: Coronal Disturbances, ed. G. A. Newkirk, 57, 105

Kopp, R. A., & Pneuman, G. W. 1976, Sol. Phys., 50, 85

Kosovichev, A. G. 2011, ApJ, 734, L15

Kosovichev, A. G., & Zharkova, V. V. 2001, ApJ, 550, L105

Lemen, J. R., et al. 2012, Sol. Phys., 275, 17

Lin, R. P., et al. 2002, Sol. Phys., 210, 3

Machado, M. E., Avrett, E. H., Vernazza, J. E., & Noyes, R. W. 1980, ApJ, 242, 336

Martínez Oliveros, J. C., et al. 2011, Sol. Phys., 269, 269

Masuda, S., Kosugi, T., & Hudson, H. S. 2001, Sol. Phys., 204, 55

Maurya, R. A. 2010, PhD thesis, Udaipur Solar Observatory, Physical Research Laboratory, India

Maurya, R. A., & Ambastha, A. 2008, *J. Astrophys. Astron.*, 29, 103

—. 2009, Sol. Phys., 258, 31

Maurya, R. A., & Ambastha, A. 2010a, in Astrophys. Space Sci. Proc., Magnetic Coupling between the Interior and the Atmosphere of the Sun,, ed. S.S. Hasan and R.J. Rutten (Berlin: Springer), 517

—. 2010b, Sol. Phys., 262, 337

Patterson, A. 1984, ApJ, 280, 884

Patterson, A., & Zirin, H. 1981, ApJ, 243, L99

Qiu, J., & Gary, D. E. 2003, ApJ, 599, 615

Schou, J., et al. 2012, Sol. Phys., 275, 29

Sturrock, P. A. 1966, Nature, 211, 695

Tsuneta, S., et al. 2008, Sol. Phys., 249, 167

Venkatakrishnan, P., Kumar, B., & Uddin, W. 2008, MNRAS, 387, L69

Vernazza, J. E., Avrett, E. H., & Loeser, R. 1981, ApJS, 45, 635

Wang, H. 2006, ApJ, 649, 490

Wang, H., Varsik, J., Zirin, H., Canfield, R. C., Leka, K. D., & Wang, J. 1992, Sol. Phys., 142, 11

Zharkova, V. V., & Zharkov, S. I. 2007, ApJ, 664, 573

Zhou, T., Ji, H., & Huang, G. 2008, *Ann. Rev. Astron. Astrophys.*, 41, 1195

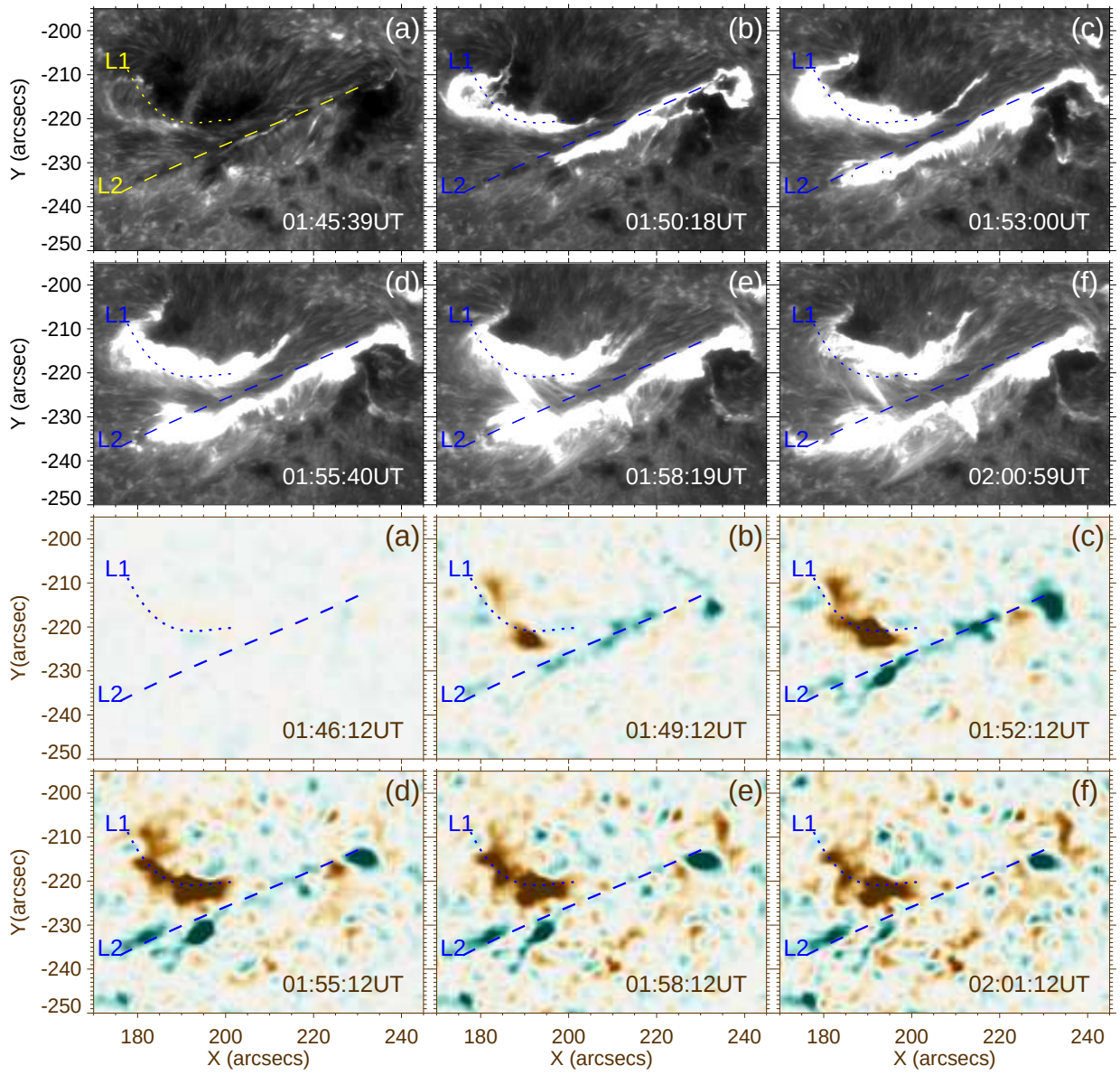

Fig. 1.— (Top two rows): CaII H filtergrams showing the spatio-temporal development of the two-ribbon X2.2 flare in AR NOAA 11158 on 2011 February 15. (Bottom two rows): Consecutive difference images of HMI magnetograms showing the enhanced "magnetic transient" features associated with the flare during the same period as above. Dotted and dashed curves marked by L1 and L2 represent the locations of the transients, drawn for reference, during the impulsive phase of the flare at 01:53 UT .

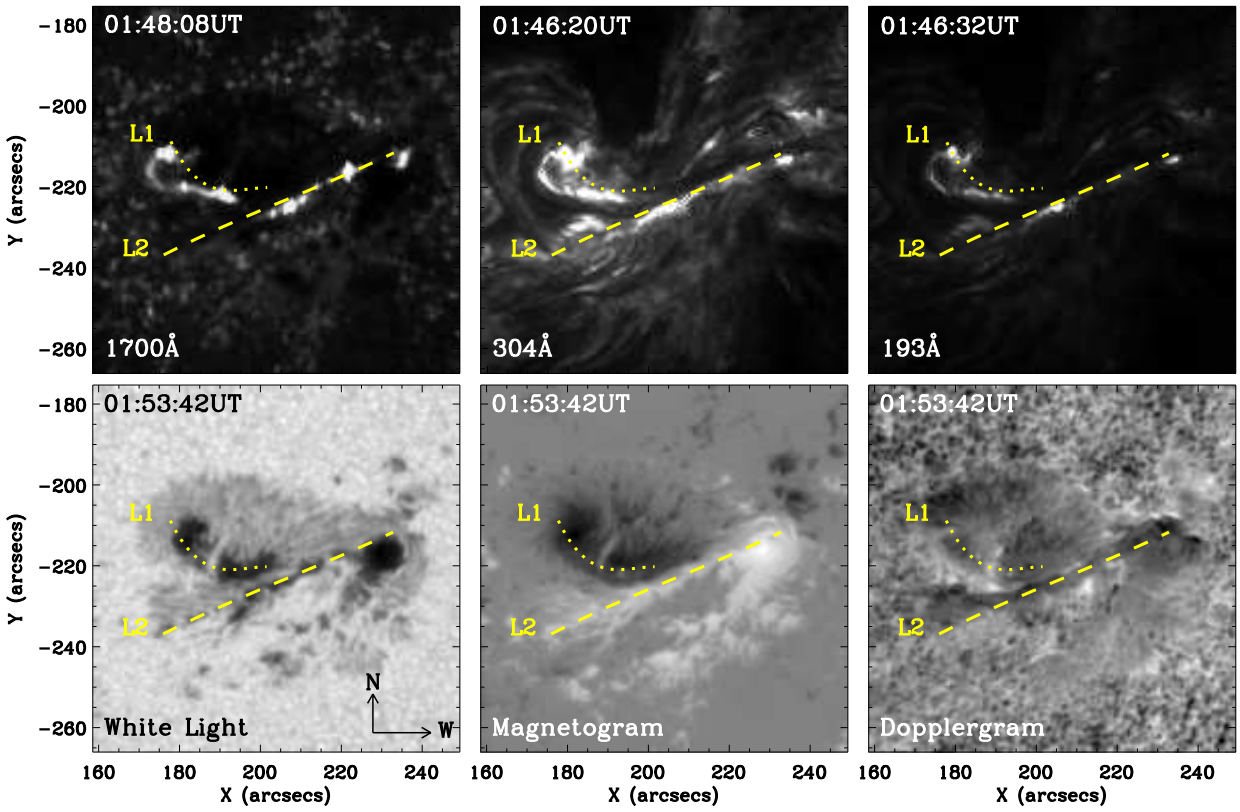

Fig. 2.— AR NOAA 11158 during the X2.2 flare of 2011 February 15. *Top (from left to right):* AIA images in the wavelengths 1700, 304 and 193Å. *Bottom (from left to right):* HMI white-light, magnetogram and dopplergram images. Dotted and dashed curves marked by L1 and L2 represent the locations of the transients, drawn for reference, during the impulsive phase of the flare at 01:53 UT.

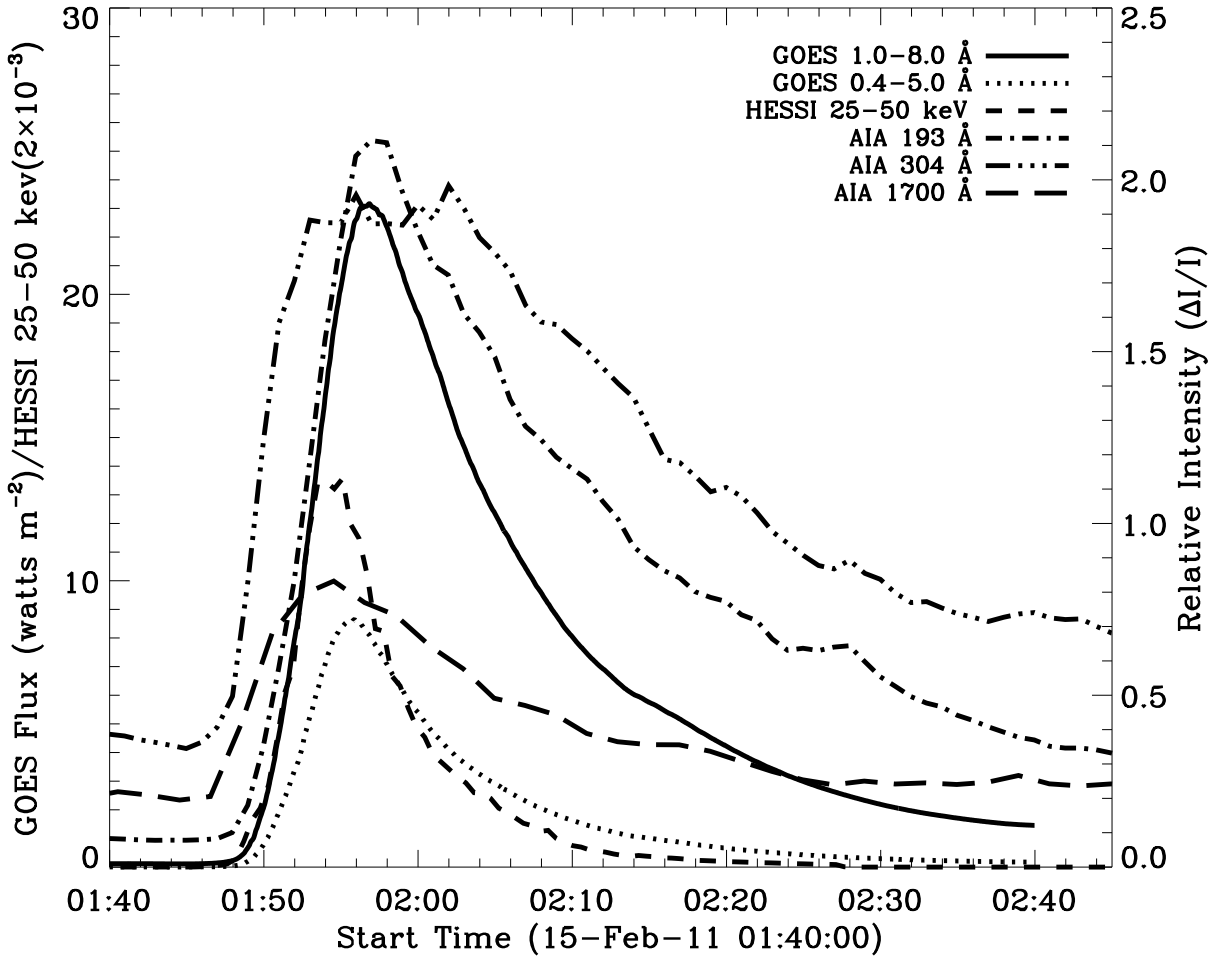

Fig. 3.— Intensity profiles of the X2.2 flare of 2011 February 15 in different wavelengths.

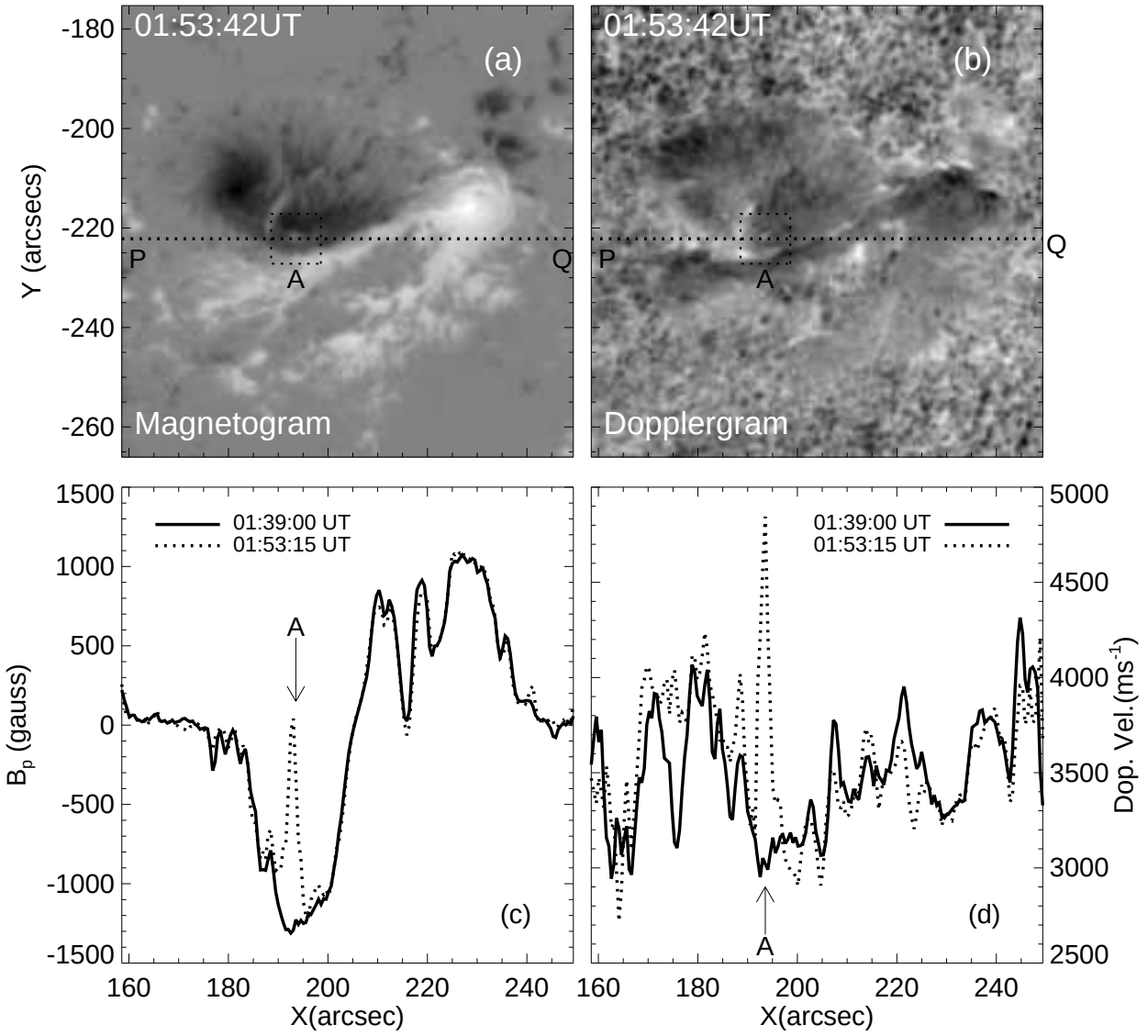

Fig. 4.— AR NOAA 11158 at the peak phase of the X2.2 flare of 2011 February 15: (a) the magnetogram, and (b) the dopplergram. The box labeled by "A" marks the area where TFs were observed. The bottom panels (c) and (d) show the corresponding profiles along the line PQ at the pre- and peak-phases of the flare represented by solid and dotted curves, respectively.

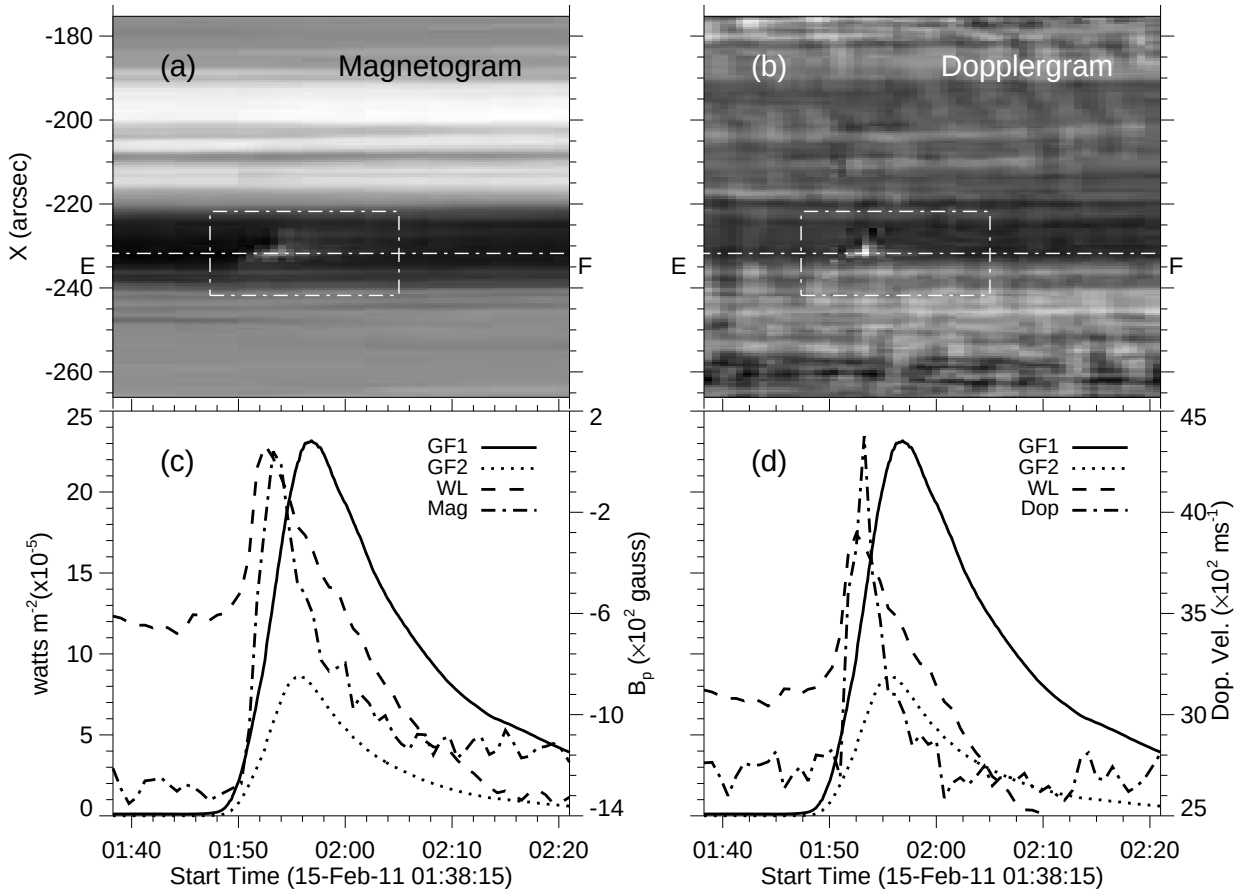

Fig. 5.— Space-time maps of (a) magnetic flux, and (b) Doppler velocity along the line PQ of Figure 4(a-b). The boxes enclose the ranges of time and location of the TFs seen during the flare. Corresponding bottom panels show the dashed-dotted profiles along the line EF for (c) magnetic flux, and (d) Doppler velocity. Also plotted are the WLF intensity (dashed), integrated GOES flux GF1(GF2) in the wavelength range 1.0–8.0(0.5–4.0)Å represented by solid (dotted) curves.

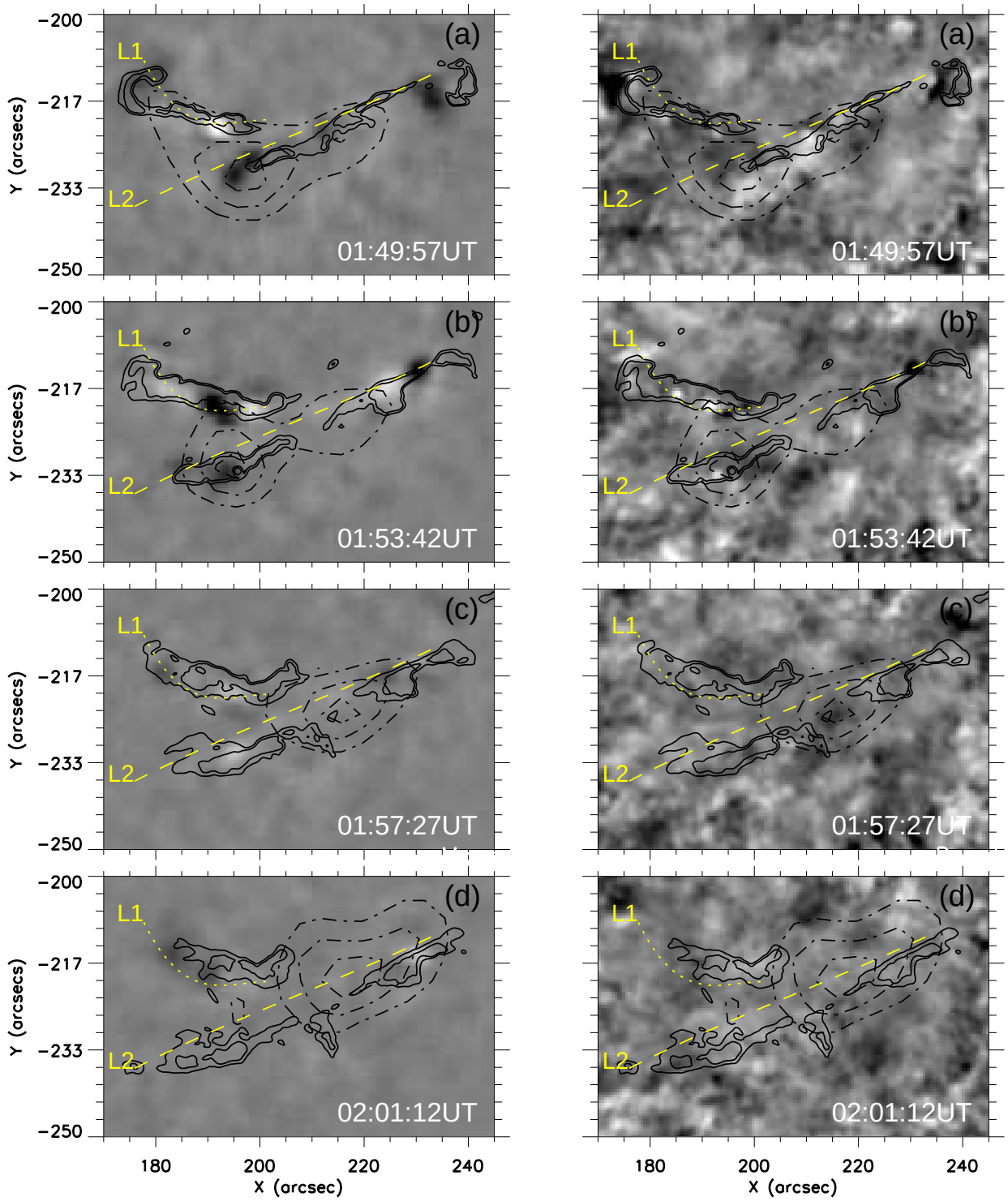

Fig. 6.— Temporal sequence of consecutive difference images: (left column) HMI magnetogram, and (right column) Dopplergram with overlaid RHESSI HXR (dashed dotted) and CaII H flare intensity (solid) contours. L1 and L2 represent the reference locations of the TFs at 01:53 UT.

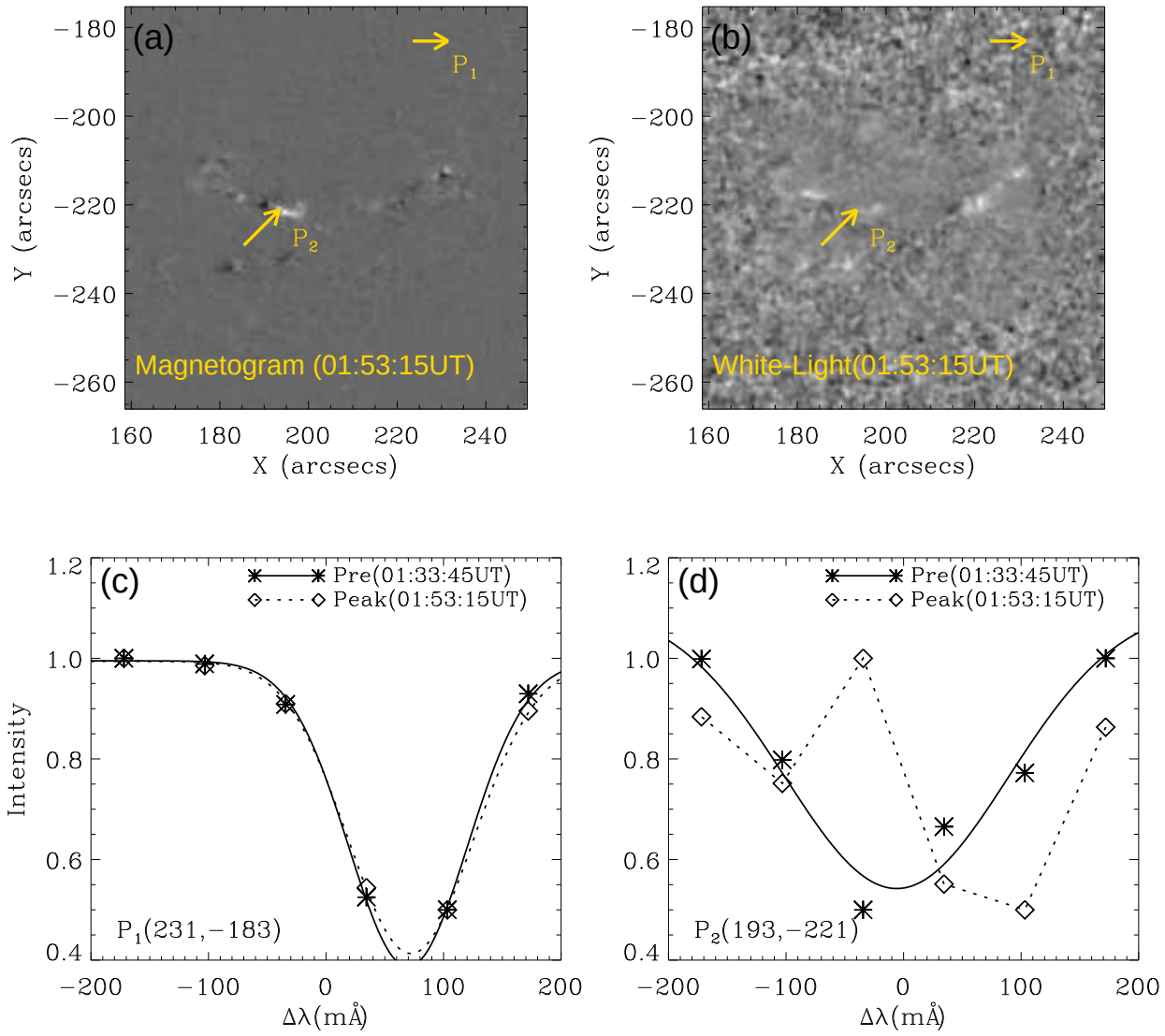

Fig. 7.— Difference images of AR NOAA 11158 - (a) magnetogram, and (b)Doppler velocity obtained at the peak phase (01:53:15 UT) of the flare with the pre-flare phase (01:33:45 UT). LCP profiles of the Fe I line in (c) P_1 (quiet), and (d) P_2 (transient) correspond to the locations marked by arrows in the top panel. The profiles are shown for the pre (01:33:45 UT) and peak (01:53:15 UT) phases, respectively by solid and dotted curves, obtained from a four parameter Gaussian fitting of the six wavelength positions, except for the peak phase at P_2.

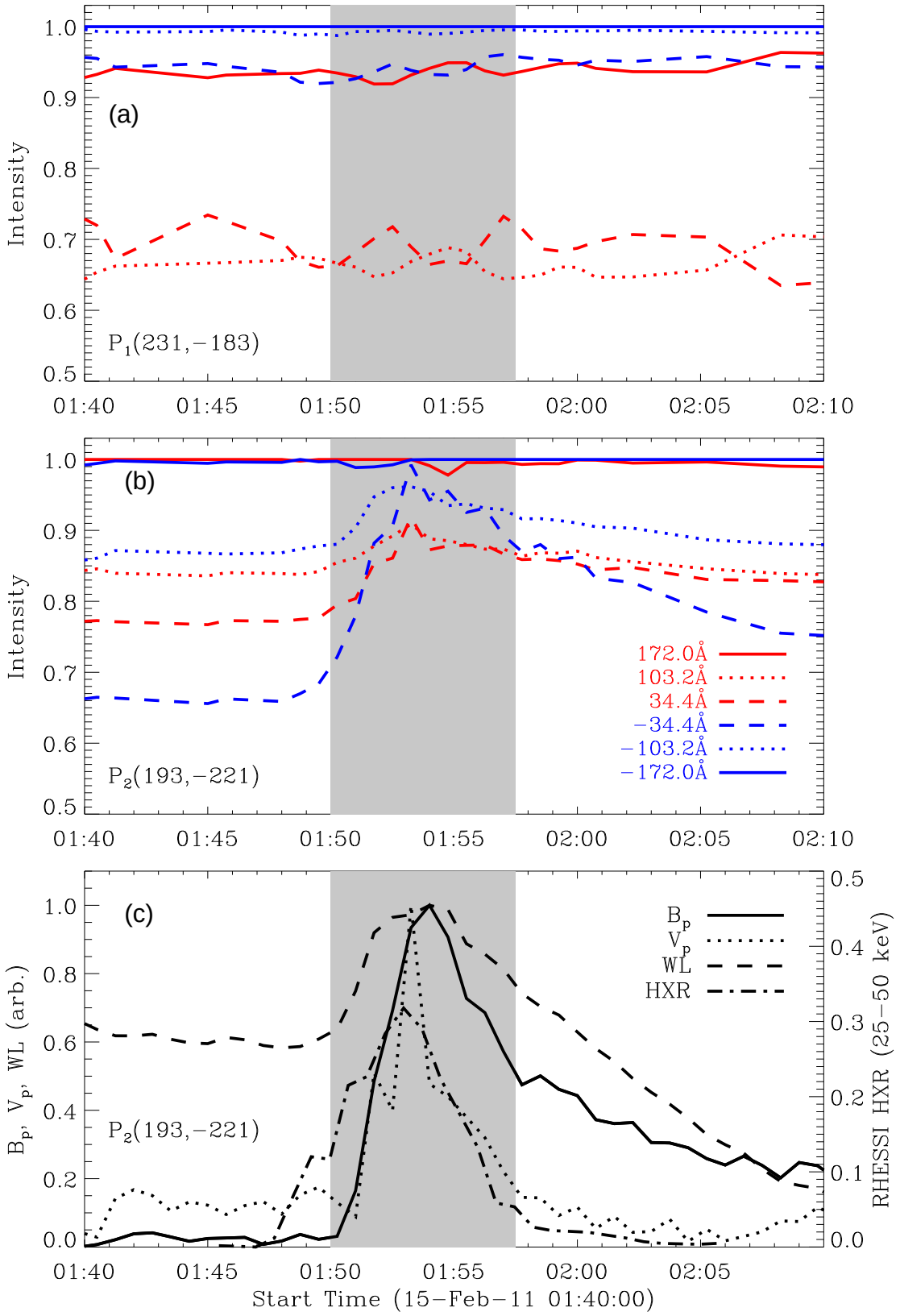

Fig. 8.— Temporal variation of normalized LCP intensities at the six wavelength positions of the Fe I line for the locations (a) P_1 and (b) P_2 (see Figure 7a, b). The corresponding variations in the photospheric magnetic flux (B_p), Doppler velocity V_p, white light intensity (WL) and RHESSI HXR energy at the location P_2 are shown in (c).

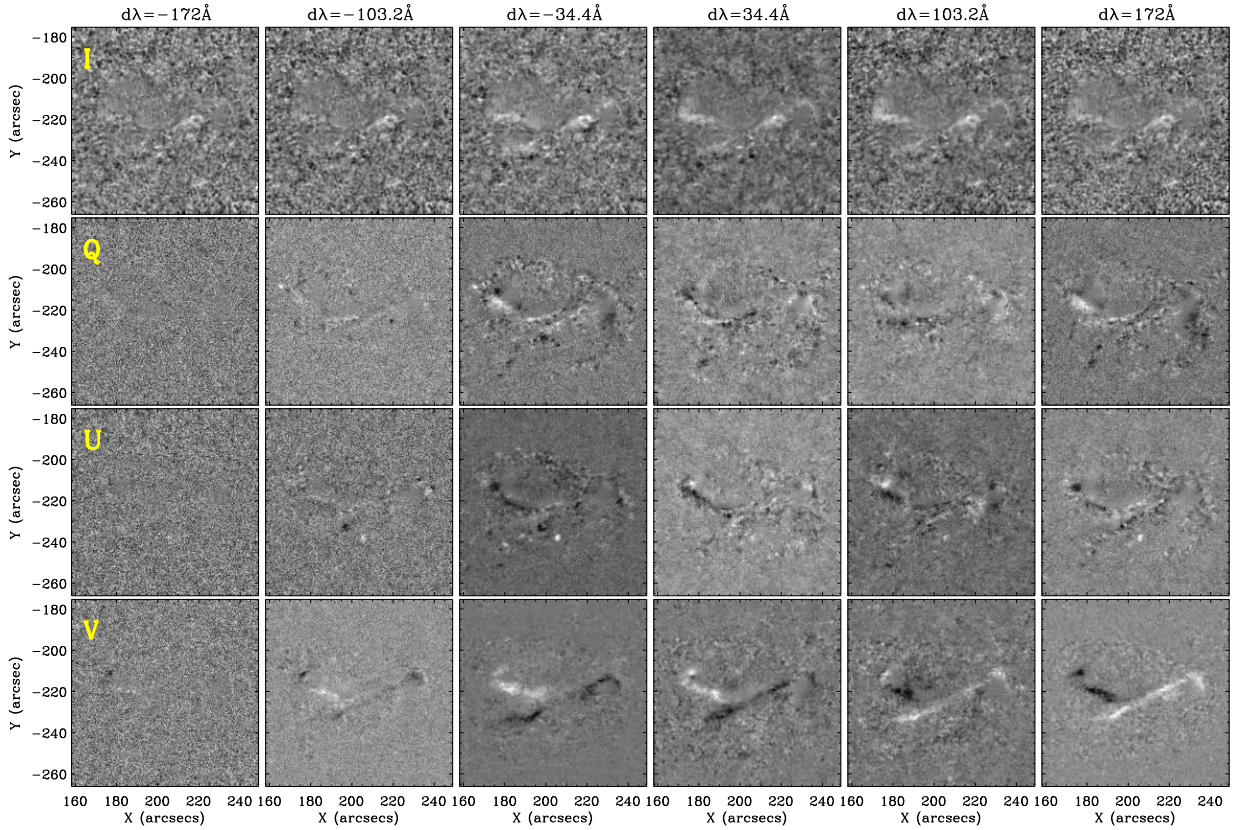

Fig. 9.— Difference maps of the AR NOAA 11158 corresponding to the Stokes parameters I, Q, U and V (from top to bottom rows) at the six HMI wavelength positions (from left to right) at the peak phase (01:52:30 UT) of the flare from the pre-flare phase (01:45:45 UT).

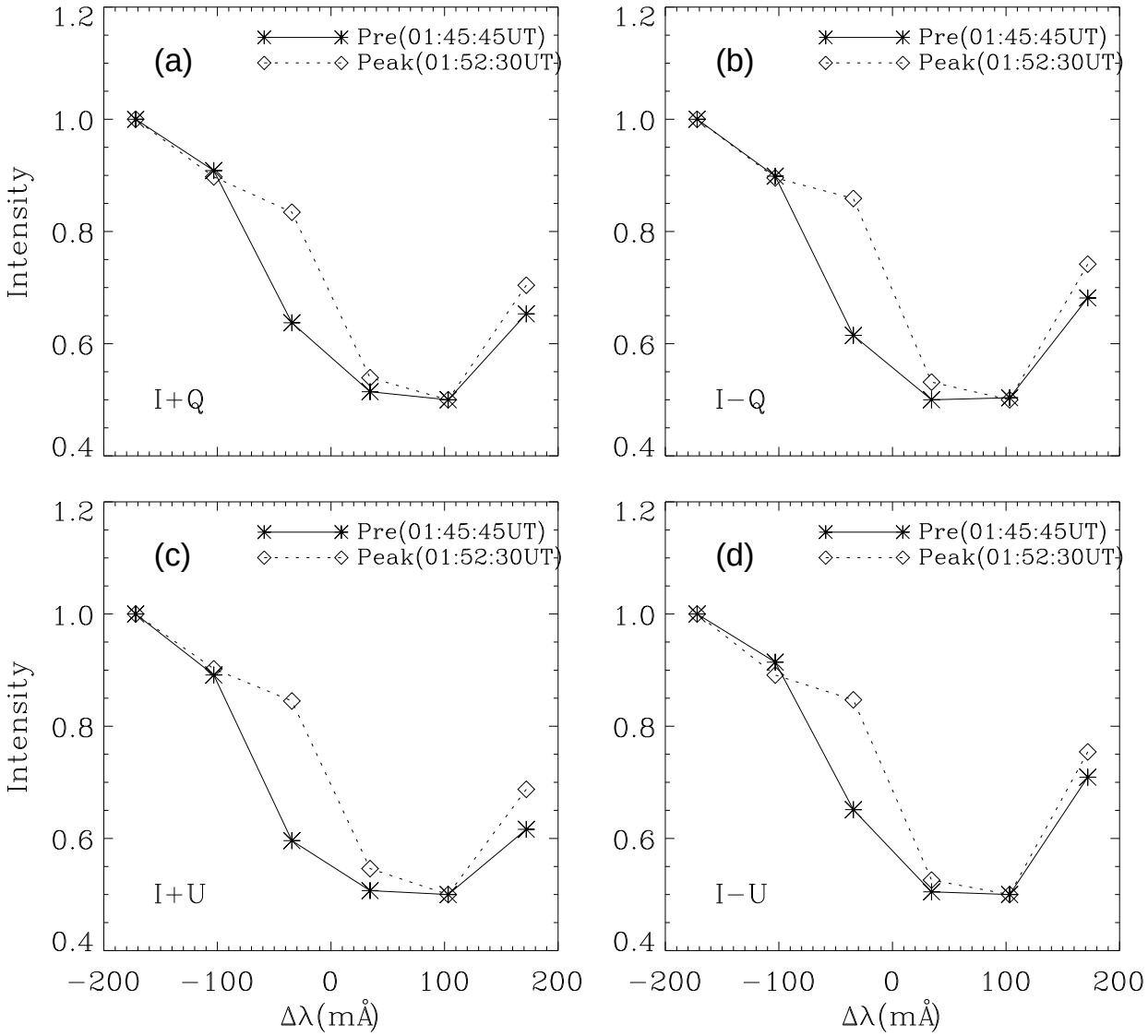

Fig. 10.— Stokes profiles at the location P2 (see Figure7(a)), where solid (dotted) curves represent the spectral profiles during the pre (peak) phase of the flare.